Next Materials 9 (2025) 101229

Contents lists available at ScienceDirect

Next Materials

journal homepage: www.sciencedirect.com/journal/next-materials

Research article

Broadband microwave absorption and improved electromagnetic performance of iron oxide–activated carbon hybrid composites in the Ku-band

Murtala Alhaji Bello [a,d], Raba'ah Syahidah Azis [a,b,*], Nurul Asiya Nadhirah Binti Yusmadi [a], Ismayadi Ismail [b], Muhammad Kashfi Shabdin [a], Nurul Huda Osman [a], Abubakar Yakubu [c], Yusuf Sani [e]

[a] Department of Physics, Faculty of Science, University Putra Malaysia, UPM, Serdang, Selangor 43400, Malaysia
[b] Nanomaterials Synthesis and Characterization Laboratory (NSCL), Institute of Nanoscience and Nanotechnology, Universiti Putra Malaysia, UPM, Serdang, Selangor 43400, Malaysia
[c] Department of Physics, Kebbi State University of Science and Technology, Aliero, Nigeria
[d] Department of Physics, Shehu Shagari College of Education, Sokoto, Nigeria
[e] Department of Pure and Applied Physics, Federal University Wukari, Nigeria

ARTICLE INFO

Keywords:
Reflection loss
Impedance matching
Saturation magnetization
Permittivity

ABSTRACT

This study explores the enhancement of microwave absorption properties in iron oxide (IO) composites through the incorporation of bio-waste-derived activated carbon (AC). Composite materials were synthesized using a cost-effective ball-milling method, combining commercially sourced activated carbon and iron oxide. The addition of highly conductive activated carbon to the ferrite matrix significantly improved reflection loss due to enhanced interfacial polarization. The dielectric permittivity and dielectric loss tangent of IO also increased with the introduction of AC. To evaluate their microwave absorption performance, the composites were embedded in epoxy resin and fabricated into single-layer structures with a 2 mm thickness. The IO/AC hybrid composite demonstrated exceptional microwave absorption, exceeding 99.9 % efficiency, with a minimum reflection loss of −39.09 dB and an absorption bandwidth of 5.28 GHz in the Ku-band region. This research introduces the novel application of bio-waste-derived activated carbon for enhancing the microwave absorption efficiency of iron oxide. The findings highlight a sustainable and cost-effective approach for developing high-performance electromagnetic wave absorbers, contributing to waste reduction and environmental sustainability.

1. Introduction

Microwave absorbing materials (MAMs) are critical in mitigating electromagnetic pollution, protecting human health, and advancing stealth technologies, particularly in military sectors [1–3]. Research into MAMs has expanded due to their broad applicability in both civil and defense industries, with growing interest in developing thin, highly efficient, and broadband absorbers that meet modern technological demands [4,5]. MAM design strategies include physically combining different absorbent materials [6], chemically modifying absorbers [7], and developing advanced single-layer structures [8]. The performance of MAMs is heavily influenced by their dimensional structures. Bulk 3D materials like ferrites [9], 2D materials such as graphene [10,11], and 1D materials like carbon nanotubes [12] each offer distinct advantages for enhancing microwave absorption capabilities. These structures impact crucial factors like surface area, interfacial polarization, and electromagnetic wave scattering, which ultimately determine the material's absorption efficiency.

For effective microwave absorption, MAMs must meet two critical criteria: (1) achieving impedance matching with the surrounding environment [13] and (2) effectively reducing the intensity of incident electromagnetic waves [14]. Impedance matching depends on the interaction between complex permittivity (ε) and complex permeability (μ), which control the material's ability to store and dissipate electric and magnetic energy. For optimal absorption, the material's permittivity and permeability must be balanced with those of free space to

* Corresponding author at: Department of Physics, Faculty of Science, University Putra Malaysia, UPM, Serdang, Selangor 43400, Malaysia.
E-mail address: rabaah@upm.edu.my (R. Syahidah Azis).

https://doi.org/10.1016/j.nxmate.2025.101229
Received 13 March 2025; Received in revised form 12 September 2025; Accepted 15 September 2025
Available online 26 September 2025

minimize reflections [15]. Materials with high permittivity but low permeability tend to reflect incident waves due to high surface resistance, while materials with high permeability but low permittivity allow waves to pass through with minimal attenuation [16].

A thorough review of the literature underscores the importance of simultaneously tuning permittivity and permeability to achieve effective electromagnetic wave absorption. Carbon-based fillers, such as carbon nanotubes, graphene, and activated carbon, are frequently used to enhance permittivity, while magnetic materials like ferrites improve permeability [17]. The synergistic combination of these materials allows for better impedance matching, enabling both electric and magnetic losses to contribute to absorption. Recent studies have demonstrated that adjusting the ratio of carbon and magnetic fillers can fine-tune these properties, leading to enhanced performance over a broad frequency range [18,19]. Balancing permittivity and permeability are particularly important for radar absorption and electromagnetic interference (EMI) shielding, where efficient wave attenuation and broad frequency response are essential. This study exemplifies this approach by hybridizing iron oxide (Fe_2O_3) with activated carbon to optimize the magnetic and dielectric properties of the composite for improved absorption performance across the microwave spectrum.

Iron oxide (Fe_2O_3) has gained attention for its potential in electromagnetic wave absorption applications. Although Fe_2O_3 has lower magnetic permeability than other magnetic materials, it contributes to electromagnetic wave attenuation through different magnetic loss mechanisms [20]. Its small particle size enhances interfacial polarization, enabling multiple reflections of electromagnetic waves [21]. Incorporating Fe_2O_3 with other materials has been shown to improve its absorption properties. For instance, Huang et al. [22] demonstrated that Fe_3O_4/MWCNT/Fe_2O_3 composites synthesized via hydrothermal methods achieved enhanced microwave absorption by adjusting the MWCNT content. Similarly, Lu et al. [23] developed CuS/γ-Fe_2O_3 van der Waals heterostructures, where γ- Fe_2O_3 nanoparticles are embedded between CuS nanosheets to optimize dielectric and magnetic losses, although bandwidth limitations persist.

Activated carbon (AC) is another widely recognized material for electromagnetic absorption due to its high electrical conductivity, which facilitates wave dissipation [24]. Its large surface area also enhances the interaction between fillers and the matrix, improving overall absorption efficiency [25]. In this study, a spinel Fe_2O_3/coconut shell-based activated carbon (AC) composite was synthesized to evaluate its microwave absorption capabilities. The composite features a carbon layer and periodic Fe_2O_3 morphology, with high-energy ball milling (HEBM) used to fine-tune its magnetic and conductive properties. The hybrid material demonstrated improved electromagnetic wave absorption due to better energy transfer between the Fe_2O_3 and AC phases.

This research bridges the gap between theoretical models and practical applications by highlighting the synergistic effects of combining carbon-based and magnetic fillers. The IO/AC hybrid composites exhibit promising broad-frequency absorption potential, making them ideal candidates for radar absorption and EMI shielding. The study provides insights into optimizing structure-property relationships, contributing to the development of advanced MAMs for both civil and military applications.

2. Material and experiments

2.1. Material

IO was supplied by Alfa Aesar, with a particle size ranging from 50 to 100 nm and a purity of 99 %. The coconut shell-derived activated carbon (activated coal), characterized by low-volume pores, was obtained from PT Cahaya Indo Abadi, Indonesia. It has an average particle diameter of less than 10 μm, a purity exceeding 97 %, and a surface area greater than 240 m^2/g.

2.2. Synthesis and composite preparation

To prepare the IO powder, a high-energy ball milling (HEBM) process was used with the 700 rpm SPEX 8000D milling machine at a ball-to-powder ratio of 10:1 for 9 h. Both vials contained equal amounts of IO powder (5 g each) along with steel balls. Each vial held 9 steel balls ranging in size from 1.6 to 0.8 cm. After the initial milling, the IO powder was mixed with AC at varying mass percentages. The mixture was first homogenized using a pestle and mortar and then subjected to an additional 30-minute milling via HEBM. For composite fabrication, the milled IO powder was mixed with AC and blended with epoxy resin (Araldite 506, Sigma Aldrich) and hardener (EpoxiCure 2, Buehler) in a 70:30 wt ratio. The mixture was uniformly combined using a mini vortex mixer at 3000 rpm for 30 min. The final composite mixtures of IO/AC, with weight ratios of 80:20, 60:40, 40:60 and 20:80, were then placed into Ku-band rectangular waveguide sample holders measuring 23×10 mm with a consistent thickness of 2 mm. The composites were left to dry at room temperature for 24 h.

2.3. Characterization

X-ray diffraction (XRD) analysis was conducted at room temperature using a Philips X′pert Diffractometer (Model PW 3040/60 MPD X'pert High Pro, Panalytical, Almelo, Netherlands) over a 2θ range of 20°–80°. The magnetic properties of the samples were evaluated at room temperature with a vibrating sample magnetometer (VSM) (Model Lakeshore 7404, Ohio, USA) under a maximum magnetic field of 10 kOe. The size, microstructure, and morphology of the nanoparticles were examined using a Field Emission Scanning Electron Microscope (FESEM) (Model FEI Nova Nano 230, USA). The FESEM system was equipped with an energy dispersive X-ray spectroscopy (EDS) system (Oxford Instrument, Model Max 20) for elemental analysis. Raman spectra were acquired using a Raman spectrometer (Witec, Oxford Instrument, Model Alpha 300 R, Germany). The electromagnetic wave absorption performance was tested using an Agilent Vector Network Analyzer (VNA) (Model N5227A, California, USA) over the Ku-band frequency range of 12–18 GHz, with a sample thickness of 2 mm. Measurements were conducted using the transmission/reflection line method in a rectangular waveguide setup.

3. Results and discussions

The X-ray diffraction (XRD) analysis of the as-synthesized iron oxide (IO) nanoparticles, depicted in Fig. 1(a), reveals that prolonged milling, up to 9 h, leads to increased peak broadening. This broadening suggests a reduction in crystallite size while maintaining the original phase of IO. Such particle diffusion is likely due to the introduction of thermodynamic energy, defects, and atomic dislocations during the milling process [26–28]. The XRD analysis of the synthesized iron oxide (IO) nanoparticles reveals distinct diffraction peaks at 2θ values of 24.64°, 33.28°, 35.86°, 40.97°, 42.92°, 49.92°, 54.04°, 58.01°, 62.46°, and 64.47°, corresponding to the (012), (104), (110), (113), (202), (024), (116), (018), (214), and (300) planes, respectively. These peaks align with the standard reference pattern for hematite (α-Fe_2O_3), specifically ICPDS card no. 98–006–9763, confirming the formation of a single-phase hematite structure. The absence of additional peaks indicates high phase purity. The average crystallite size, calculated using the Debye–Scherrer equation, is approximately 11.02 nm, suggesting nanocrystalline characteristics. Notably, the electrical and magnetic properties of such complex oxides are influenced by both the average crystallite size and its distribution [29,30].

Fig. 1(b) presents the XRD pattern of the bio-waste-derived activated carbon (AC), the XRD pattern exhibits broad peaks at 2θ values of 27.47° and 42.67°, corresponding to the (002) and (100) planes of graphitic carbon, respectively, consistent with ICPDS card no. 74–2330. The broad nature of these peaks indicates an amorphous or poorly crystalline

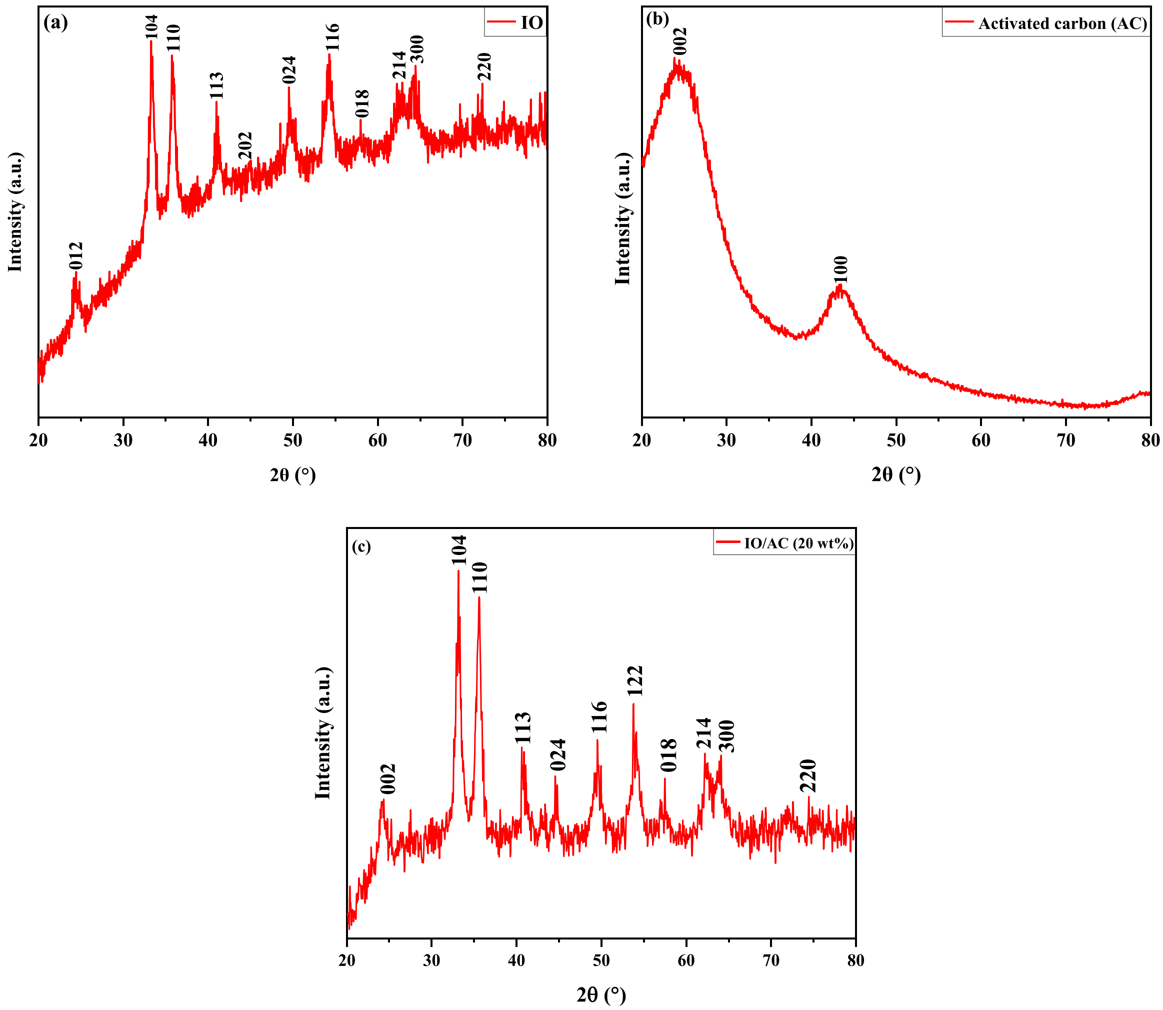

Fig. 1. Illustrates the X-ray diffraction (XRD) patterns of (a) IO (b) AC and (c) the IO/AC hybrid composite.

structure, typical of activated carbon materials [31,32]. In the IO/AC composite shown in Fig. 1(c), the XRD pattern predominantly reflects the characteristic peaks of α-Fe_2O_3, with no significant shifts in peak positions, suggesting that the incorporation of activated carbon does not alter the hematite phase. However, a noticeable bump near $2\theta = 24.14^{\circ}$ indicates the presence of amorphous carbon within the composite matrix. The ball milling was employed to enhance the dispersion of iron oxide within the composite matrix. XRD analysis Fig. 1(c) shows that the characteristic diffraction peaks of iron oxide remained intact after milling, indicating that no phase transformation occurred. However, a slight broadening of the peaks suggests a reduction in crystallite size, which is consistent with FESEM observations of particle distribution. This size reduction is beneficial for improving the interfacial interaction between iron oxide and the activated carbon, potentially enhancing electromagnetic wave absorption performance. When it comes to environmental stability, previous research indicates that carbon matrices can serve as protective barriers for iron oxide nanoparticles [33]. They help shield these nanoparticles from oxidation, which in turn helps maintain their magnetic and electromagnetic properties over time. This implies that the IO/AC composites not only enjoy better dispersion and interfacial polarization but also provide improved long-term stability, all thanks to the protective function of activated carbon.

In order to determine the effect of activated carbon incorporation on the magnetic properties of iron oxide, the saturation magnetization and coercivity of the produced composites were analyzed. The magnetic hysteresis loops for the IO and hybrid composite of IO and IO/AC were obtained using the VSM technique and are shown in Fig. 2. The

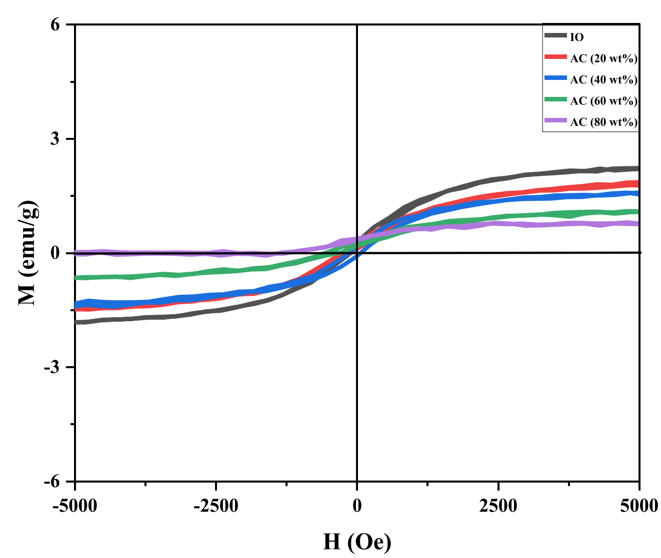

Fig. 2. M-H hysteresis graph for IO and IO/AC hybrid composites.

maximum saturation magnetization of pure iron oxide is 2.2402 emu/g. However, as activated carbon is added, the saturation magnetization gradually decreases. The IO/AC hybrid composite exhibits a saturation magnetization value of 1.6488 emu/g. As reported in a previous study

[34], this decrease in saturation magnetization is likely due to the decrease in the net magnetic moment caused by the incorporation of magnetic ferrite with nonmagnetic activated carbon. Remarkably, the hysteresis loops reveal an increase in the coercivity (Hc) of the composite with the addition of AC. This enhancement in Hc can be attributed to increased surface anisotropy and pinning effects at the interfaces between IO nanoparticles and AC, which hinder domain wall motion.

Qualitatively, the magnetic losses in microwave absorption mainly come from factors like natural (ferromagnetic) resonance and eddy current loss. When saturation magnetization (Ms) increases, it boosts a material's magnetic permeability, especially the imaginary part (μ''), which results in greater energy dissipation when exposed to an alternating electromagnetic field—this ultimately enhances absorption efficiency. Moreover, coercivity (Hc) plays a role in determining the resonant frequency of absorption: based on ferromagnetic resonance theory, a higher Hc raises the resonance frequency, helping to align absorption peaks with the operational band. In the case of IO/AC composites, the changes in Ms and Hc due to AC incorporation not only affect magnetic losses but also modify resonance behavior, leading to improved microwave absorption performance through better-optimized magnetic loss mechanisms.

The bias shown in the magnetic hysteresis loops of IO and IO/AC composites may be attributed to multiple factors. The exchange bias effect, which results from the interaction of ferromagnetic and antiferromagnetic phases, may lead to a shift in the hysteretic loop [35,36]. Additionally, nanoparticle size, distribution, and surface effects, as well as magnetocrystalline anisotropy, all play significant roles [37]. Surface changes and interactions between IO and AC can have a further impact on magnetic properties. The bias can also be influenced by defects at the interface between iron oxide and activated carbon, strain-induced anisotropy, and interfacial exchange coupling between different magnetic phases. The bias is evident in the magnetic hysteresis loops of AC (80 wt%) and AC (60 wt%), but it is not clearly observed in other samples. This suggests that at certain AC concentrations, the interactions between the magnetic and nonmagnetic components become more pronounced, leading to an observable shift in the hysteresis loop [38]. A particularly intriguing observation is that the magnetization of AC (80 wt%) is zero in the range of 1200–5000 Oe. The AC (80 wt%) composite's zero magnetization in the 1200–5000 Oe range is principally owing to the superparamagnetic character of the iron oxide nanoparticles, which are influenced due to their nanoscale size [39], and their interaction with the effects of its activated carbon matrix.

The VSM results also indicate that tuning the ratio of Fe_2O_3 to activated carbon can effectively control the permeability and permittivity of the composite, allowing for better impedance matching. This finding corroborates the theoretical models that suggest a careful balance between permittivity and permeability is essential for optimizing microwave absorption performance [40]. High crystallinity and phase purity, as evidenced by sharp and well-defined peaks, increase the dielectric properties of IO/AC composites by enhancing polarization and reducing dielectric loss. The identification of various iron oxide phases informs magnetic behavior, with different phases improving coercivity and saturation magnetization. Although direct interface analysis via TEM or XPS was not conducted in this study, the heterogeneous structure observed in FESEM and the frequency-dependent dielectric relaxation behavior (Fig. 5) are indicative of interface polarization effects, consistent with previous reports [41].

The structure and surface morphology of milled iron oxide (IO),

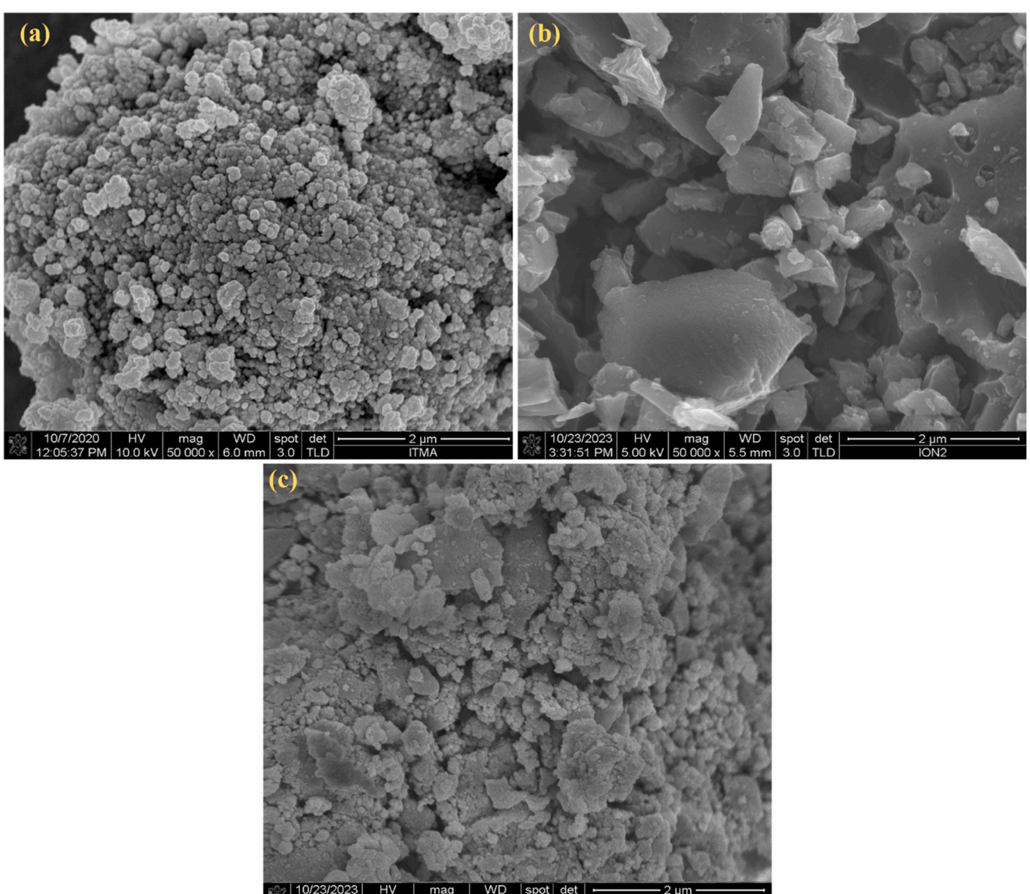

Fig. 3. Presents FESEM micrographs illustrating (a) IO nanoparticles milled for 9 h, (b) a highly porous activated carbon powder, and (c) the IO/AC hybrid composite.

activated carbon (AC), and AC (20 wt%) hybrid composites were analyzed using field emission scanning electron microscopy (FESEM), as shown in Fig. 3. The FESEM micrograph of iron oxide (IO) (Fig. 3a) reveals the presence of predominantly spherical particles. This morphology is characteristic of IO nanoparticles, which often exhibit irregular shapes and non-uniform distribution, consistent with previous findings [42]. The spherical morphology of IO nanoparticles plays a crucial role in enhancing electromagnetic wave absorption by providing a larger surface area, promoting multiple reflections and scattering, improving impedance matching, and potentially inducing resonance and polarization effects [43,44]. Additionally, the high-energy ball milling process resulted in nanoparticles with a uniform size distribution, with an average particle size of 15.4 nm. The smaller particle sizes, as observed in the FESEM images, further enhance interfacial polarization due to the increased surface area, thereby leading to higher microwave attenuation [45]. Additionally, the high-energy ball milling process resulted in nanoparticles with a uniform size distribution, with an average particle size of 15.4 nm. The smaller particle sizes, as observed in the FESEM images, further enhance interfacial polarization due to the increased surface area, thereby leading to higher microwave attenuation [46].

The FESEM micrograph of activated carbon (Fig. 3b) reveals a uniform and facetted surface structure. The facetted morphology suggests the presence of distinct crystalline facets, which generally contribute to a larger surface area, thereby enhancing the material's absorption capacity. This structured morphology is particularly beneficial for

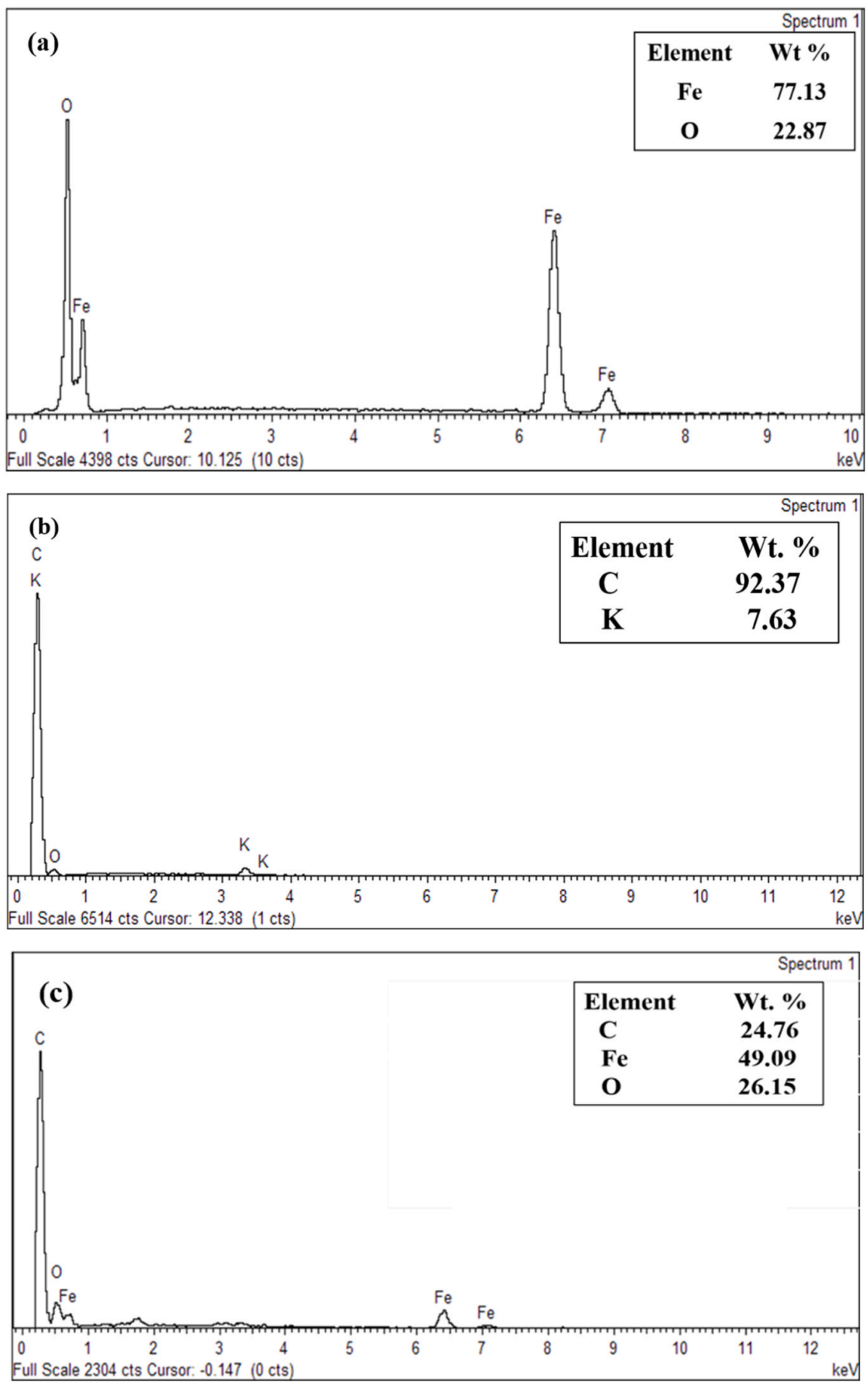

Fig. 4. EDX pattern of (a) IO (b) AC and (b) IO/AC hybrid composites.

microwave absorption applications, as the exposed facets provide active sites for chemical interactions [47,48].

The FESEM micrograph of the AC (20 wt%) hybrid composite (Fig. 3c) clearly displays the coexistence of spherical-like IO particles alongside the facetted activated carbon matrix, confirming the successful formation of the IO/AC nanocomposite. The morphology of the IO/AC composite differs significantly from that of pure IO and AC, indicating enhanced microwave absorption performance due to increased surface area, improved interfacial interactions, and synergistic effects between magnetic and dielectric properties. These structural features facilitate multiple reflections, enhanced impedance matching, and effective loss mechanisms, thereby leading to higher microwave absorption over a wider frequency range.

Quantitative elemental analysis was performed on iron oxide (IO), activated carbon (AC), and their hybrid composite (IO/AC) using energy-dispersive X-ray spectroscopy (EDX) to validate the chemical composition of these samples (Fig. 4(a)–c). The EDX spectrum for Fe_2O_3 nanoparticles (Fig. 4a) displays prominent peaks corresponding to iron (Fe) and oxygen (O), with no detectable impurities, indicating high purity. The analysis reveals average elemental contents of approximately 77.13 % Fe and 22.87 % O in the IO powders.

In contrast, the EDX results for AC powders (Fig. 4b) show dominant peaks for carbon (C) and potassium (K), with average contents of approximately 92.37 % C and 7.63 % K. The presence of potassium is likely due to the activation process used during the synthesis of the activated carbon.

For the IO/AC hybrid composite (Fig. 4c), the EDX analysis indicates the presence of Fe, O, and C, with average contents of approximately 49.09 % Fe, 26.15 % O, and 24.76 % C. No other elemental contaminants were detected, suggesting successful integration of Fe_2O_3 and AC without introducing impurities. These findings confirm the effective synthesis of the IO/AC composite, combining the magnetic properties of iron oxide with the conductive nature of activated carbon

Raman spectroscopy is a widely used technique for analyzing the microstructure of carbonaceous materials. It consistently reveals two prominent bands: the D band at approximately 1350 cm^{-1} and the G band at around 1600 cm^{-1} . The D band is associated with structural disorder and arises from the disorder-induced breathing mode with A_1g symmetry, involving phonons near the K zone boundary. In contrast, the G band corresponds to zone-center phonons with E_2g symmetry, which are related to the stretching of sp^2-hybridized carbon atoms [49]. A crucial parameter in Raman analysis is the intensity ratio of the D band to the G band (I_D/I_G), commonly used to evaluate the defect density in carbon-based materials. For the IO/AC hybrid composites, an I_D/I_G value of 1.00 was obtained (Fig. 5). This suggests that the incorporation of magnetic particles significantly increases defect density [50],), which, in turn, facilitates the formation of additional polarization centers. The enhanced defect density contributes to stronger dielectric loss, thereby improving the material's effectiveness in attenuating incident electromagnetic waves [51,52]. Additionally, the observed vibrational modes associated with Fe–O stretching align with theoretical expectations, indicating that the Fe_2O_3 phase is well-incorporated and actively contributes to magnetic losses, a key mechanism for microwave absorption [9]. These structural and vibrational properties play a crucial role in enhancing microwave absorption by facilitating interfacial polarization and multiple reflections of electromagnetic waves, as predicted by theory [53]. Furthermore, previous studies have demonstrated that structural defects in activated carbon (AC) serve as polarization centers, playing a crucial role in microwave absorption performance [54]. This finding reinforces the potential of IO/AC hybrid composites for applications requiring efficient electromagnetic wave absorption.

Further, the permittivity and permeability graphs were employed to analyze the composite's electrical and magnetic behavior as a function of frequency. The real and imaginary parts of the complex permittivity ($\varepsilon = \varepsilon' - j\varepsilon''$) and complex permeability ($\mu = \mu' - j\mu''$) provide insights into how electromagnetic (EM) energy is stored and lost, respectively [55–57]. For microwave absorption applications, high losses are desirable to reduce the energy of incident EM waves, whereas high dielectric materials are typically used in energy storage devices [58]. Figs. 6 and 7 (a, b) shows the ε', ε'', μ', and μ'' of IO/AC. They can be represented by the

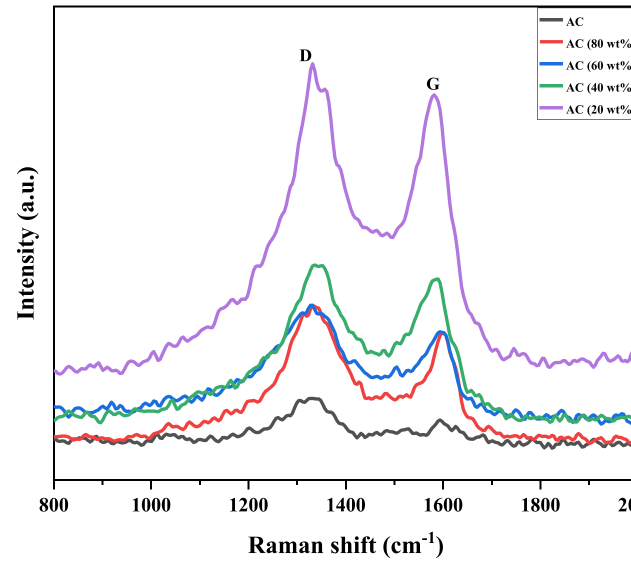

Fig. 5. Displays the Raman spectrum of the AC and IO/AC hybrid composites.

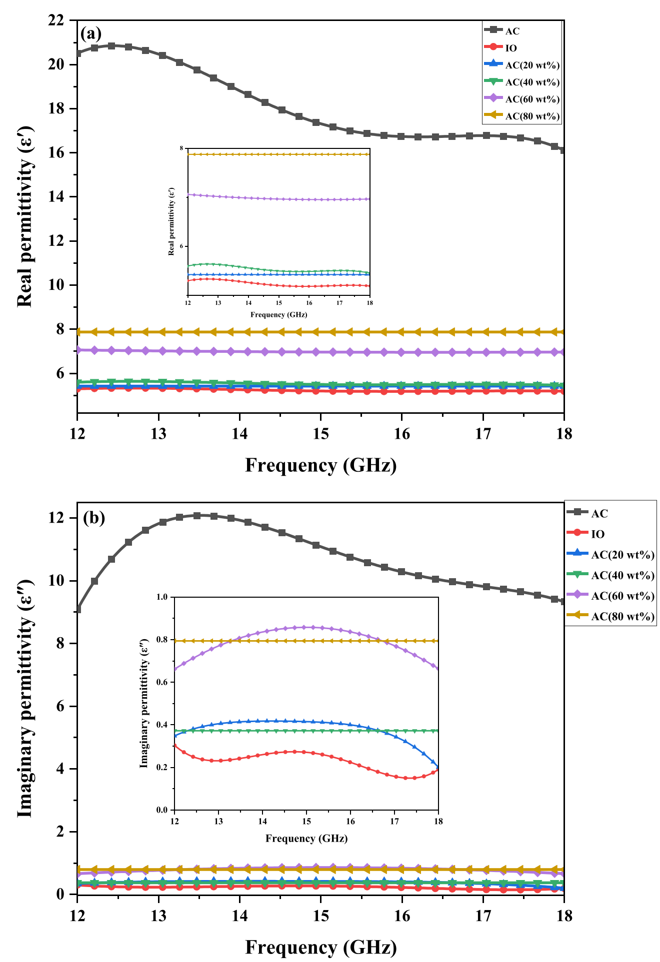

Fig. 6. Variation in the Ku-band electrical permittivity of IO/AC hybrid composites in the (a) real and (b) imaginary parts with different filler contents (20, 40, 60, and 80 wt%) and a thickness of *d* = 2 mm.

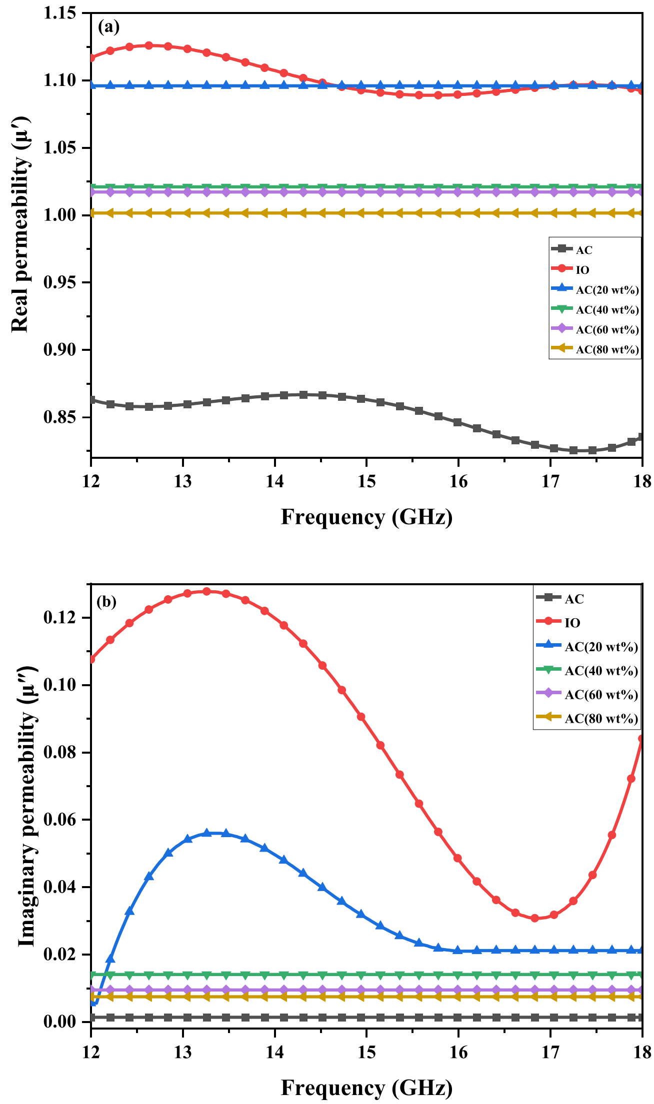

Fig. 7. Variation in the Ku-band magnetic permeability of IO/AC hybrid composites in the (a) real and (b) imaginary parts with different filler contents (20, 40, 60, and 80 wt%) and a thickness of $d = 2$ mm.

following equation [59,60]:

$$\varepsilon_\tau = \varepsilon_\infty + \frac{\varepsilon_s - \varepsilon_\infty}{1 + j2\pi f\tau} \quad (1)$$

$$\varepsilon' = \varepsilon_\infty + \frac{\varepsilon_s - \varepsilon_\infty}{1 + (2\pi f)^2 \tau^2} \quad (2)$$

$$\varepsilon'' = \frac{2\pi f\tau(\varepsilon_s - \varepsilon_\infty)}{1 + (2\pi f)^2 \tau^2} \quad (3)$$

$$\mu' = 1 + \frac{M}{H}\cos\theta \quad (4)$$

$$\mu'' = 1 + \frac{M}{H}\sin\theta \quad (5)$$

The real and imaginary parts of electrical permittivity as a function of frequency are shown in Fig. 6. Both ε′ and ε″ exhibit an upward trend with increasing activated carbon concentration in the composite. This behavior is attributed to the high electrical conductivity of activated carbon, which improves the charge transport characteristics of the system. Furthermore, in line with the Maxwell–Wagner effect, interfacial polarization occurs at the boundaries between iron oxide and carbon phases, creating regions of charge accumulation that enhance dielectric response [61,62]. Such interfacial polarization is a key microwave absorption mechanism, as it leads to dipolar relaxation, converting EM wave energy into heat.

The observed increase of the dielectric loss factor, or ε″, directly contributes to the attenuation of microwave energy through a number of absorption modes, including as conductive loss, dipolar polarization, and interfacial polarization. Activated carbon is added to the iron oxide matrix to produce conductive networks that enable free charge flow, which causes resistive losses and localized heating. If combined together, these elements improve the composite's ability to attenuate electromagnetic waves. The material's use in microwave absorption and electromagnetic interference (EMI) shielding is thereby supported by an improvement in the overall dielectric loss behavior, particularly in the Ku-band frequency range.

The frequency-dependent behavior of the real (μ′) and imaginary (μ″) components of complex permeability (μ_r) for IO, AC, and IO/AC hybrid composites is presented in Fig. 7. The results show that activated carbon (AC), being non-magnetic, has negligible influence on the magnetic response of the composite, while iron oxide (IO) retains dominant magnetic behavior. The imaginary permeability (μ″), which reflects magnetic loss, is highest in the IO and 20 wt% AC composites, suggesting strong magnetic energy dissipation. These magnetic losses primarily arising from hysteresis, eddy current loss, and magnetic resonance are essential mechanisms in microwave absorption [63–65]. At lower AC content (e.g., 20 wt%), the magnetic IO particles maintain strong coupling, enabling effective domain wall motion and interfacial polarization. This promotes enhanced hysteresis and relaxation losses, leading to increased imaginary permeability and stronger absorption. However, with increasing AC content, the IO particles become diluted within the non-magnetic matrix, disrupting the magnetic pathways and reducing energy dissipation. This leads to diminished magnetic losses and weaker absorption efficiency at higher filler concentrations. Therefore, the 20 wt% IO/AC composite strikes an optimal balance between magnetic and dielectric contributions, making it a promising candidate for efficient microwave absorption in the Ku-band.

To further analyze the energy dissipation mechanisms in the fabricated composites, the dielectric and magnetic loss tangent curves were derived. These parameters quantify the energy loss due to polarization relaxation and magnetic domain movement, respectively, and are defined as follows [66]:

$$tan\delta_e = \frac{\varepsilon''}{\varepsilon'} \quad (6)$$

$$tan\delta_m = \frac{\mu''}{\mu'} \quad (7)$$

Where, tan δ_e (dielectric loss tangent) accounts for the conversion of electromagnetic energy into heat through dipole relaxation, conduction loss, and interfacial polarization [67], while tan δ_m (magnetic loss tangent) reflects the dissipation of magnetic energy due to domain wall resonance, eddy current loss, and spin relaxation [68]. These loss parameters are essential indicators of the material's ability to absorb and dissipate electromagnetic energy rather than reflect it.

The dielectric and magnetic loss tangent curves for IO/AC hybrid composites with varying activated carbon (AC) content at a thickness of 2 mm are depicted in Fig. 8. The dielectric loss tangent curves shown in Fig. 8(a) mirror the behavior of imaginary permittivity (ε″), with tan δ_e peaking at 0.64 for 80 wt% AC, indicating that AC substantially contributes to dielectric losses through enhanced interfacial polarization and electrical conductivity. Meanwhile, Fig. 8(b) illustrates the magnetic loss tangent, where pure IO shows a higher tan δ_m value (~0.11 at 13.23 GHz), which confirms strong magnetic loss mechanisms such as natural resonance and hysteresis loss. Table 1 summarizes the mean

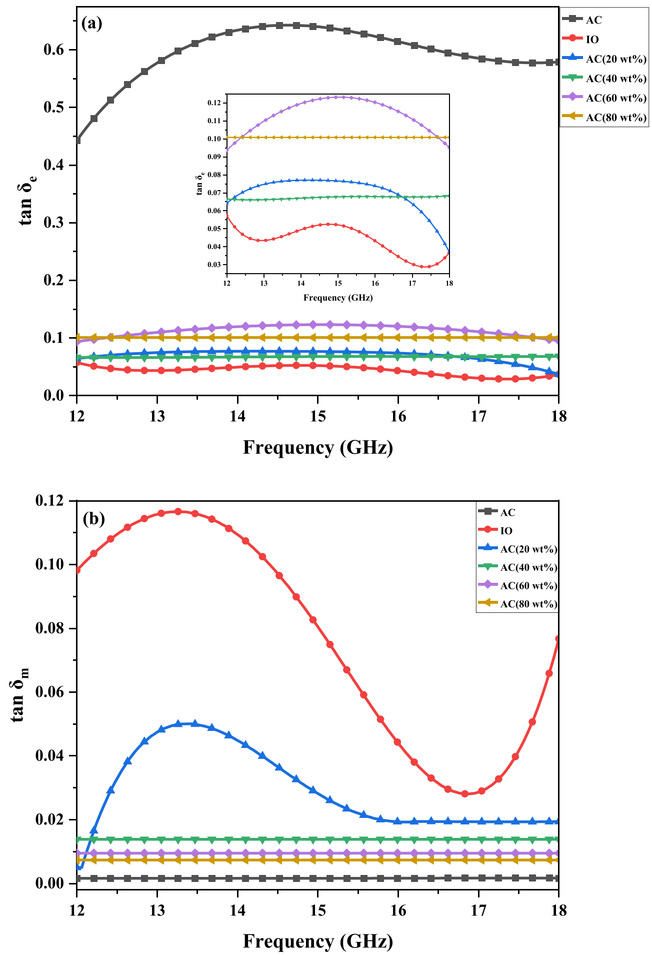

Fig. 8. Depicts the curves for (a) dielectric loss tangent and (b) magnetic loss tangent of the IO/AC hybrid composites with different filler contents (20, 40, 60, and 80 wt%) and a thickness of $d = 2$ mm.

Table 1
The permittivity, permeability, and loss tangent values for IO/AC hybrid composites.

Sample Type	ε' (mean)	ε'' (mean)	μ' (mean)	μ'' (mean)	$\tan\delta_e$ (mean)	$\tan\delta_m$ (mean)
Fe_2O_3	5.23	0.23	1.1028	0.0840	0.04	0.0293
Activated Carbon	18.08	10.78	0.8511	0.0014	0.58	0.0016
AC (20 %)	5.42	0.38	1.0960	0.0324	0.07	0.0767
AC (40 %)	5.70	0.37	1.0016	0.0075	0.01	0.0138
AC (60 %)	7.24	0.79	1.0210	0.0141	0.1135	0.0094
AC (80 %)	8.23	0.79	1.0172	0.0095	0.1008	0.0073

values of electrical permittivity, magnetic permeability, and loss tangents for IO, AC, and IO/AC composites with varying AC content (20 – 80 wt%).

Among these materials, IO, being inherently magnetic, exhibits the highest magnetic losses, while activated carbon, as a non-magnetic material, shows the lowest values. The AC (20 wt%) composite retains a mean magnetic loss value close to pure IO, suggesting that IO's magnetic properties remain dominant at low AC content. However, as AC content increases (40 – 80 wt%), the mean magnetic loss values progressively decrease, indicating that higher AC concentrations dilute the magnetic properties of IO. This reduction weakens magnetic coupling and energy dissipation mechanisms in the composites, highlighting the trade-off between enhancing dielectric losses and preserving magnetic loss contributions in microwave absorption applications.

The amount of electromagnetic energy reflected from a material surface, known as reflection loss (RL), is a critical parameter in evaluating microwave absorption efficiency. Minimizing RL ensures greater absorption of incident electromagnetic (EM) waves, which is essential for applications such as electromagnetic interference (EMI) shielding and stealth technology. The RL can be calculated using the relative permittivity and permeability values, as expressed by the following equation [69,70]:

$$RL = 20\log_{10}\left|\frac{Z_{in} - Z_o}{Z_{in} + Z_o}\right| \tag{8}$$

where Z_o represents the impedance of free space (with a value of 120π), while Z_{in} denotes the input impedance of the material or surface interface, given by:

$$Z_{in} = Z_o\sqrt{\frac{\mu_r'}{\varepsilon_r'}}\tanh\left[j\ \frac{2\pi}{c}\ \sqrt{\mu_r'\varepsilon_r'}\ \ fd\right] \tag{9}$$

μ_r represents the relative permeability, ε_r stands for the relative permittivity, c denotes the speed of light, f signifies the operating frequency, and d corresponds to the thickness of the absorber.

According to Eq. (8), an RL minimum value of −10 dB implies that 10 % of the energy is reflected, while 90 % of the incident energy is absorbed [71,72]. Likewise, an RL value of −20 dB indicates that only 1 % of the incident energy is reflected, meaning 99 % of the incident electromagnetic (EM) wave energy is absorbed.

In practical applications, an effective microwave absorber should achieve an RL minimum of −10 dB or lower, ensuring substantial energy absorption and minimal reflection. This principle is critical for designing materials for radar stealth technology, electromagnetic shielding, and wave attenuation in communication systems. By optimizing parameters such as material composition, filler content, and structural design, researchers can tailor RL values to meet specific application requirements.

Using Eq. (8), the reflection loss (RL) values of the composites were obtained by varying the thickness of the pellets from 1 to 3 mm. The RL curves, plotted in Fig. 9 as a function of frequency, reveal a distinct trend. Initially, the absorption peak increases from −2.28 dB for pure Fe_2O_3 to −39.09 dB for the AC (20 wt%) composite, indicating a highly efficient microwave absorption behavior. However, beyond this point, the RL values decrease as the AC content increases from 20–80 wt%. Compared to graphene/$Fe_{50}Ni_{50}$ composites [73], which exhibit excellent electromagnetic wave absorption properties but suffer from high production costs and limited scalability, the IO/AC composites synthesized in this study demonstrate competitive performance (reflection loss of −39.09 dB at 15.03 GHz) with additional benefits of sustainability

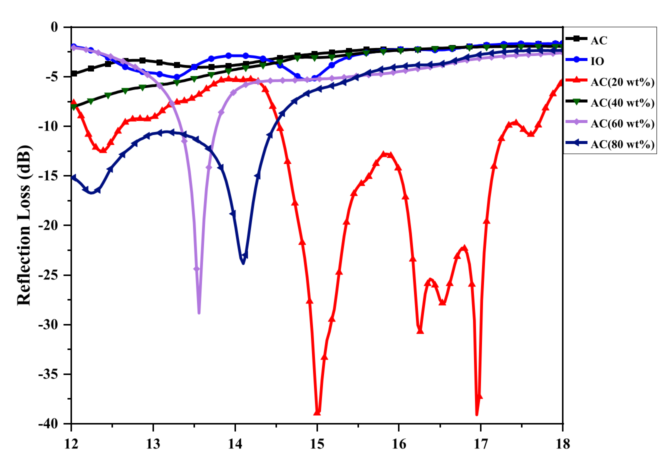

Fig. 9. Displays the reflection loss curves for IO/AC hybrid composites with different filler contents (20, 40, 60, and 80 wt%) and a thickness of $d = 2$ mm.

and cost-efficiency. Activated carbon, derived from abundant biomass sources, provides an environmentally friendly and economically viable alternative to graphene, making it more suitable for large-scale industrial applications.

To further validate the superior absorption performance of the AC (20 wt%) composite, the effective absorption bandwidth (EAB) was analyzed. This composite exhibits an EAB of 5.28 GHz, covering the frequency range of 13.45–18.73 GHz, which is significantly broader than that of pure Fe_2O_3 (0.60 GHz) and other AC composites. The enhanced absorption can be attributed to synergistic effects of optimized impedance matching and multiple loss mechanisms. Impedance matching ensures minimal reflection at the air–material interface by tuning the relative balance between permittivity and permeability, allowing maximum electromagnetic wave entry into the material. Dielectric losses are enhanced by the activated carbon via interfacial polarization, dipole polarization, and conduction losses, which arise from abundant functional groups and defects. Magnetic losses, provided by Fe_2O_3, stem from natural resonance, eddy current loss, and possibly domain wall resonance, contributing to broader absorption over a wider frequency range. The multiple reflections and scattering at porous interfaces and heterogeneous phase boundaries in the composite further increase the path length and energy dissipation of incident waves. Together, these mechanisms result in deep and broad microwave absorption, as evidenced by the significant RL and EAB values. These findings align with previous studies, such as on $Co_{0.5}Ni_{0.5}Fe_2O_4$ fibers/reduced graphene oxide composites, where a thickness of 2.0 mm resulted in a minimum RL of −14.7 dB at 12.9 GHz [74], underscoring the critical role of thickness and compositional synergy in microwave attenuation.

A comparative analysis with higher AC content (40–80 wt%) shows a decline in RL values due to excessive permittivity, which leads to impedance mismatch and increased surface reflection, rather than effective wave penetration and attenuation. The AC (80 wt%) and AC (60 wt%) composites exhibit strong surface reflections at high frequencies, resulting in diminished absorption efficiency [75].

The exceptional absorption performance of the AC (20 wt%) composite is further explained by its satisfaction of the quarter-wavelength matching condition, as determined by Eq. (10). The calculated effective thickness of 2 mm at 16.95 GHz is consistent with experimental observations, reinforcing the material's ability to achieve destructive interference between incident and reflected waves a key mechanism in wave cancellation and absorption enhancement. Furthermore, the AC (20 wt%) hybrid composite demonstrates superior microwave absorption due to its synergistic balance of dielectric and magnetic losses, enhanced interfacial polarization, and optimal attenuation constant, all contributing to its broadband performance. The increased number of heterointerfaces between the AC and Fe_2O_3 phases likely facilitate Maxwell–Wagner-type interfacial polarization, a dominant loss mechanism in heterogeneous composites. This promotes space charge accumulation, which in turn boosts energy dissipation through multiple scattering and relaxation processes. Moreover, it is evident that the reflection loss curve of AC (20 wt%) has shifted to higher frequencies, indicating that the material structure supports high-frequency EM wave phase cancellation within the Ku-band [76]. This phase cancellation occurs when the impedance of the absorber matches that of free space, ensuring minimal reflection and maximum absorption. The effective coating thickness (d) of the absorber material must satisfy the following relationship, derived from the quarter-wavelength theory for optimized absorption [77]:

$$d = \frac{nc}{4f\sqrt{|\varepsilon_r||\mu_r|}} \tag{10}$$

where n is an integer value (e.g., n = 1, 3, 5….), c is the speed of light in a vacuum, f is the operational frequency, ε_r is the complex permittivity, and μ_r is the complex permeability of the absorber material. The equation highlights the significance of material properties in determining the optimal thickness for effective microwave absorption. Materials with higher ε'' and μ'' values offer stronger attenuation because they promote energy loss through mechanisms such as dipole polarization, interfacial polarization, eddy current loss, and domain wall resonance. Thus, Eq. (10) highlights an inverse relationship between absorber thickness and frequency, implying that thinner materials are more effective at higher frequencies. The consistent rightward shift of the reflection loss peak toward higher frequencies with fixed thickness strongly supports the contribution of electromagnetic wave cancellation and phase-matching phenomena. This behavior is prominently observed in the AC (20 wt%) hybrid composite, which exhibits a peak reflection loss of –39.09 dB at 16.95 GHz with a thickness of 2 mm, indicating over 99.99 % microwave absorption. Such performance makes it a compelling candidate for high-frequency electromagnetic interference (EMI) shielding and stealth applications. Fig. 9 presents the reflection loss curves of IO/AC composites at 2 mm thickness, where the AC (20 wt%) sample outperforms other compositions. It not only achieves the lowest reflection loss but also delivers a broad effective absorption bandwidth (EAB), extending from 14.40 to 17.25 GHz, where RL ≤ –10 dB. This superior performance can be attributed to a synergistic enhancement in both intrinsic and extrinsic loss mechanisms, including interfacial polarization, dipole polarization, and multiple internal reflections facilitated by the porous structure and conductive pathways of activated carbon.

To further elucidate the underlying absorption mechanism, electromagnetic attenuation constant (α) and impedance matching conditions were investigated. The attenuation constant, derived from Eq. (11), is a critical parameter that quantifies the material's capability to dissipate incident EM energy through dielectric and magnetic losses [78]:

$$\alpha = \frac{\sqrt{2\pi f}}{C}\sqrt{(\mu''\varepsilon'' - \mu'\varepsilon') + \sqrt{(\mu''\varepsilon'' - \mu'\varepsilon')^2 + (\mu''\varepsilon'' - \mu'\varepsilon')^2}} \tag{11}$$

As shown in Fig. 10(a), α increases systematically with increasing AC content, especially for the AC (80 wt%) and pure AC samples, owing to their higher complex permittivity (ε' and ε''). Elevated permittivity enhances dielectric loss by promoting space charge polarization and increasing the conversion of electromagnetic energy into heat via ohmic conduction and relaxation processes [79]. However, a high attenuation constant alone does not guarantee effective absorption. Efficient impedance matching the condition under which the intrinsic impedance of the absorber approximates that of free space is equally essential to minimize wave reflection at the air-material interface. When impedance matching is achieved, more energy penetrates the absorber, where it is subsequently attenuated by internal loss mechanisms. For the AC (20 wt %) composite, the impedance is well-matched across a wide frequency range, enabling the incident wave to enter the absorber and be dissipated via combined dielectric loss (e.g., conduction loss, interfacial polarization) and multiple scattering effects due to its heterogeneous microstructure. The impedance matching of the new composites, shown in Fig. 10(b), was examined by calculating the normalized impedance (Z_{in}/Z_o) using Eq. (9). To achieve ideal impedance matching, Zin/Zo should equal 1. As anticipated, the AC (20 wt%) composite demonstrated the most effective impedance matching among all the composites developed. Additionally, the increase in electrical conductivity, from IO to AC (20 wt%), led to improved impedance matching. However, further addition of activated carbon resulted in high conductivity, which caused more reflection from the absorber's surface and, consequently, reduced impedance matching [80]. The excellent microwave absorption properties of AC (20 wt%) in the Ku-band are attributed to its attenuation constant and effective impedance matching.

In the gigahertz range, magnetic loss mechanisms in absorbing materials are predominantly attributed to eddy current loss, natural resonance, domain wall resonance, and exchange resonance. Among these, eddy current loss arises from induced circular currents within the

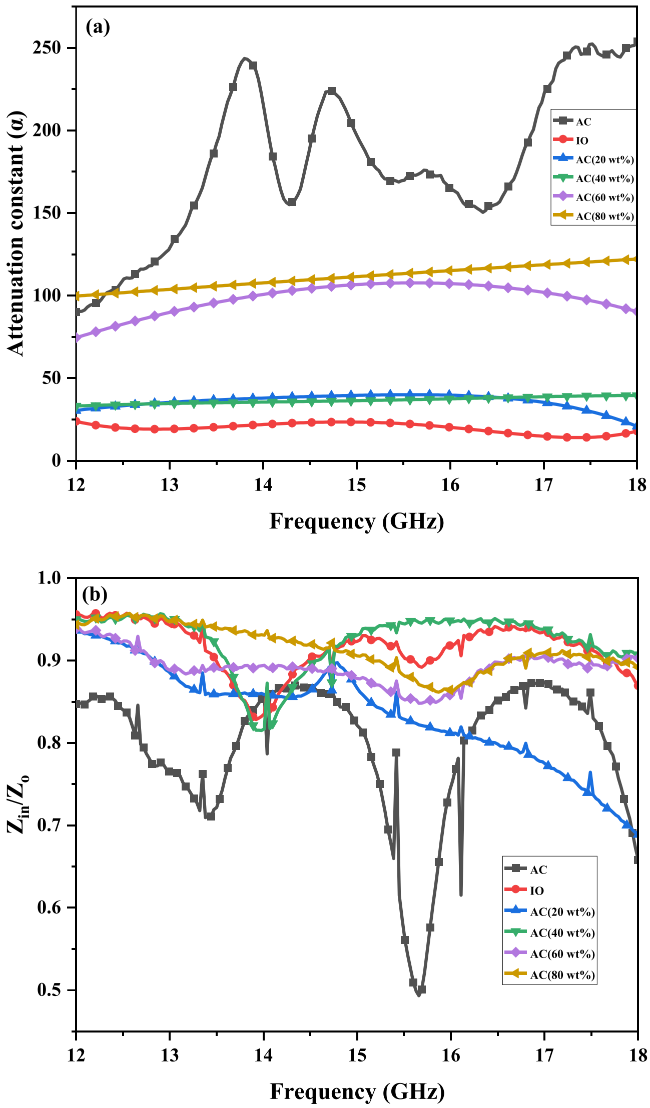

Fig. 10. Illustrates (a) the electromagnetic attenuation constant and (b) the normalized impedance plot for the IO/AC hybrid composites with different filler contents (20, 40, 60, and 80 wt%) and a thickness of $d = 2$ mm.

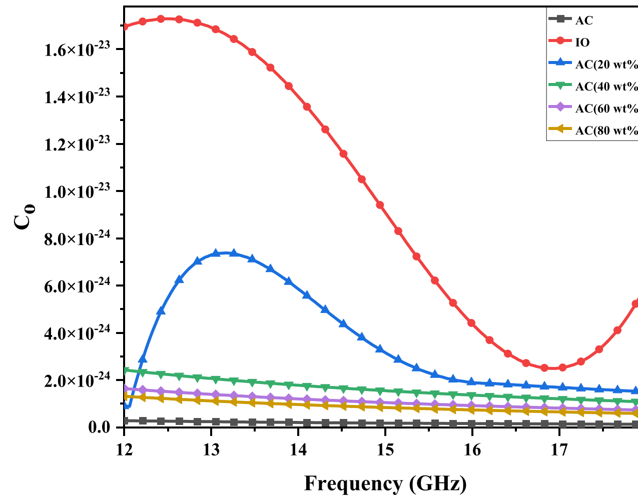

Fig. 11. Illustrates Co versus frequency of AC, IO and IO/AC hybrid composites with different filler contents (20, 40, 60, and 80 wt%) and a thickness of $d = 2$ mm.

conductive components of the composite, and its influence can be assessed using the eddy current coefficient (C_o), defined as:

$$C_0 = (\mu''(\mu')^{-2f^{-1}}) = 2\pi\mu_0 d^2\sigma \tag{12}$$

where a frequency-independent C_o suggests dominant eddy current behavior [81,82]. Fig. 11 illustrates that for IO/AC composites, especially the sample containing 20 wt% AC, the C_o values fluctuate significantly between 12 and 16 GHz, unlike other samples that maintain a relatively stable eddy current trend. This fluctuation indicates that eddy currents are not the principal contributors to magnetic loss in this system. Instead, the observed microwave absorption is more likely governed by natural resonance and exchange resonance, which are strongly dependent on particle size, anisotropy fields, and magnetic domain dynamics. Natural resonance typically dominates in the lower gigahertz range and is associated with the precession of magnetic moments in response to the alternating field, while exchange resonance occurs at higher frequencies due to magnetic interactions between adjacent atoms or nanoparticles. Additionally, interface-induced effects between the Fe_2O_3 and the activated carbon matrix can promote magnetic relaxation and localized field distortions, further enhancing energy dissipation.

In the 16–18 GHz region, the stability of the C_o values implies that non-eddy mechanisms such as spin rotation, domain wall resonance, and interfacial polarization play a dominant role in attenuating the incident electromagnetic waves. The synergy between dielectric and magnetic losses, facilitated by the heterogeneous interfaces in the IO/AC matrix, enables impedance matching, attenuation enhancement, and multiple scattering, all of which are critical to effective broadband microwave absorption. Notably, the composite demonstrates strong reflection loss (> −30 dB) and wideband absorption in the Ku-band with a minimal coating thickness, highlighting its suitability for electromagnetic interference (EMI) shielding and stealth technology applications.

4. Conclusion

A Ku-band radar absorber was successfully fabricated using iron oxide (IO) and bio-waste-derived activated carbon (AC). The IO/AC hybrid composites exhibited improved electrical behavior, with increasing AC content leading to enhanced interfacial polarization. The permittivity of IO increased from 5.53 to 7.87 upon AC incorporation, while the saturation magnetization of IO decreased from 2.2402 emu/g to 1.6488 emu/g in the AC (20 wt%) composite. The imaginary permittivity values of the IO/AC hybrid composites were significantly higher than those of pure IO, indicating a strong influence of dielectric losses on microwave absorption performance. The synergy between dielectric and magnetic losses in the IO/AC composites resulted in enhanced electromagnetic attenuation and effective impedance matching. The magnetic losses in the hybrid composites were primarily attributed to the eddy current effect. Among the synthesized materials, the AC (20 wt%) composite exhibited the highest performance, achieving a maximum reflection loss of −39.09 dB and a 99.9 % absorption bandwidth ranging from 14.40 to 17.25 GHz. These findings demonstrate that the IO/AC hybrid composites possess highly favorable magnetic and dielectric properties, making them promising candidates for microwave absorber applications. Beyond electromagnetic wave absorption, these composites also hold potential for energy storage and environmental technology applications, further broadening their scope of practical use.

CRediT authorship contribution statement

Bello Murtala Alhaji: Conceptualization, Investigation, Methodology, Data curation, Writing – Original draft, review & editing. **Raba'ah Syahidah Aziz:** Conceptualization, Funding acquisition, Supervision, Writing - review & editing, Writing – Original draft, Resources. **Nurul**

Asiya Nadhirah Binti Yusmadi: Investigation, Formal analysis, Data curation **Ismayadi Ismail:** Supervision, Writing – review & editing. **Nurul Huda Osman:** Supervision, Writing – review & editing, **Muhammad Shabdin Kashfi:** Writing – review & editing, Supervision. **Yakubu Abubakar:** Supervision, Writing – review & editing. **Yusuf Sani:** Validation, Formal analysis.

Declaration of Competing Interest

The authors declare that they have no known competing financial interests or personal relationships that could have appeared to influence the work reported in this paper.

Acknowledgements

The authors thank the Fundamental Research Grant (FRGS) with reference (FRGS/1/2023/STG07/UPM/02/8) for sponsoring this research.

Data availability

Data will be made available on request.

References

[1] H. Dong, Y. Zhang, C. Yu, Z. Wang, Y. Huang, Eco-friendly microwave absorption metastructure: design, optimization, and performance of CPVM based on PLA@CF, Chem. Eng. J. 493 (2024) 152477.
[2] M.F. Elmahaishi, R.S. Azis, I. Ismail, F.D. Muhammad, A review on electromagnetic microwave absorption properties: their materials and performance, J. Mater. Res. Technol. 20 (2022) 2188–2220.
[3] Y. Wu, S. Tan, Y. Zhao, L. Liang, M. Zhou, G. Ji, Broadband multispectral compatible absorbers for radar, infrared and visible stealth application, Prog. Mater. Sci. 135 (2023) 101088.
[4] W. Wang, Z. Li, X. Gao, Y. Huang, R. He, Material extrusion 3D printing of large-scale SiC honeycomb metastructure for ultra-broadband and high temperature electromagnetic wave absorption, Addit. Manuf. 85 (2024) 104158.
[5] X. Xiang, Z. Yang, G. Fang, Y. Tang, Y. Li, Y. Zhang, D.H. Kim, C. Liu, Tailoring tactics for optimizing microwave absorbing behaviors in ferrite materials, Mater. Today Phys. 36 (2023) 101184.
[6] J. Cheng, H. Zhang, Y. Xiong, L. Gao, B. Wen, H. Raza, H. Wang, G. Zheng, D. Zhang, H. Zhang, Construction of multiple interfaces and dielectric/magnetic heterostructures in electromagnetic wave absorbers with enhanced absorption performance: a review, J. Mater. 7 (2021) 1233–1263.
[7] K. Zhang, X. Gao, Q. Zhang, H. Chen, X. Chen, Fe3O4 nanoparticles decorated MWCNTs@C ferrite nanocomposites and their enhanced microwave absorption properties, J. Magn. Magn. Mater. 452 (2018) 55–63, https://doi.org/10.1016/j.jmmm.2017.12.039.
[8] R. Zhan, J. Zhang, Q. Gao, Q. Jia, Z. Zhang, G. Zhang, W. Gu, Microwave absorption performance of single-layer and multi-layer structures prepared by cnts/Fe_3O_4 nonwoven materials, Crystals 11 (2021).
[9] T. Hou, B. Wang, Z. Jia, H. Wu, D. Lan, Z. Huang, A. Feng, M. Ma, G. Wu, A review of metal oxide-related microwave absorbing materials from the dimension and morphology perspective, J. Mater. Sci. Mater. Electron 30 (2019) 10961–10984.
[10] Y. Zhang, P. Zhao, Q. Lu, Y. Zhang, H. Lei, C. Yu, Y. Huang, J. Yu, Functional additive manufacturing of large-size metastructure with efficient electromagnetic absorption and mechanical adaptation, Compos. Part A Appl. Sci. Manuf. 173 (2023) 106752.
[11] L. Huang, C. Chen, H.X. Zhao, J. Liu, X.X. Wang, A.-, W.-B. Liao, Z.-Y. Liu, C.-Y. Yu, Z. Li, Y. Zhang, H. Zhang, J. Lu, S. Ruan, Y.-J. Zeng, Challenges and future perspectives on microwave absorption based on two-dimensional materials and structures, Iopsci. Iop. Org. 31 (2020) 162001.
[12] C. Ding, C. Shao, S. Wu, Y. Ma, Y. Liu, S. Ma, X. Hu, Z. Cao, X. Ren, B. Zhong, G. Wen, X. Huang, A review of 1D carbon-based materials assembly design for lightweight microwave absorption, Carbon N. Y. 213 (2023) 118279.
[13] H. Shi, T. Wang, J. Cheng, H. Zhao, S. Li. Ultralow-density Carbon Foam Composites with Bean-like Co-embedded Carbon Nanotube Whiskers Towards High-performance Microwave Absorption, Elsevier, 2021, 863158090.
[14] Q. Li, Z. Zhang, L. Qi, Q. Liao, Z. Kang, Y. Zhang, Q. Li, Z. Zhang, L. Qi, Q. Liao, Z. Kang, Y. Zhang, Toward the application of high frequency electromagnetic wave absorption by carbon nanostructures, Adv. Sci. 6 (2019) 1–23, https://doi.org/10.1002/advs.201801057.
[15] B. Quan, X. Liang, G. Xu, Y. Cheng, Y. Zhang, W. Liu, G. Ji, Y. Du, A permittivity regulating strategy to achieve high-performance electromagnetic wave absorbers with compatibility of impedance matching and energy conservation, N. J. Chem. 41 (2017) 1259–1266.
[16] B. Zhao, Y. Li, Q. Zeng, L. Wang, J. Ding, R. Zhang, R. Che, Galvanic replacement reaction involving core–shell magnetic chains and orientation-tunable microwave absorption properties, Small 16 (2020) 2003502.
[17] S. Wang, H. Zhang, Q. Liu, X. Kong, Magnetic carbon nanotubes-based microwave absorbents: review and perspective, Synth. Met. 291 (2022) 117198.
[18] Y.W. Choi, U. Hwang, J.W. Ho, W. Park, T. Hassan, C.M. Koo, J.Do Nam, Y.J. Song, P.J. Yoo, Enhanced electromagnetic interference shielding in cement composites utilizing carbon fiber clustered networks with dual different lengths, Carbon N. Y 233 (2025) 119887, https://doi.org/10.1016/J.CARBON.2024.119887.
[19] I. Ismail, R.S. Azis, A review of magnetic nanocomposites for EMI shielding: synthesis, properties, and mechanisms, J. Mater. Sci. 59 (2024) 5293–5329, https://doi.org/10.1007/S10853-024-09527-2.
[20] C. Zhang, D. Wang, L. Dong, K. Li, Y. Zhang, P. Yang, S. Yi, X. Dai, C. Yin, Z. Du, X. Zhang, Q. Zhou, Z. Yi, J. Rao, Y. Zhang, Microwave absorption of α-Fe_2O_3@ diatomite composites, Int. J. Mol. Sci. 23 (2022).
[21] J. Pan, H. Guo, M. Wang, H. Yang, H. Hu, P. Liu, H. Zhu, Shape anisotropic Fe_3O_4 nanotubes for efficient microwave absorption, Nano Res. 13 (2020) 621–629.
[22] L. Huang, X. Liu, R. Yu, Enhanced microwave absorption properties of rod-shaped Fe_2O_3/Fe_3O_4/MWCNTs composites, Prog. Nat. Sci. Mater. Int. 28 (2018) 288–295, https://doi.org/10.1016/J.PNSC.2017.04.002.
[23] N. Lu, J. Xu, M. Yuan, G. Sun, Flower-like CuS/γ-Fe_2O_3 van der waals heterostructures with high-efficient electromagnetic wave absorption, Nano Res. (2023).
[24] M.M. Harussani, S.M. Sapuan, G. Nadeem, T. Rafin, W. Kirubaanand, Recent applications of carbon-based composites in defence industry: a review, Def. Technol. 18 (2022) 1281–1300.
[25] J. Lewis, M.A.Q. Al-sayaghi, C. Buelke, A. Alshami, Activated carbon in mixed-matrix membranes, Sep. Purif. Rev. 50 (2021) 1–31.
[26] B. AlMangour, D. Grzesiak, J.M. Yang, In situ formation of TiC-particle-reinforced stainless steel matrix nanocomposites during ball milling: feedstock powder preparation for selective laser melting at various energy densities, Powder Technol. 326 (2018) 467–478.
[27] A. Patra, S.K. Karak, S. Pal, Effects of mechanical alloying on solid solubility, Adv. Eng. Forum 15 (2016) 17–24.
[28] Z. Liao, A. la Monaca, J. Murray, A. Speidel, D. Ushmaev, A. Clare, D. Axinte, R. M'Saoubi, Surface integrity in metal machining - part I: fundamentals of surface characteristics and formation mechanisms, Int. J. Mach. Tools Manuf. 162 (2021) 103687.
[29] M.M.L. Sonia, S. Anand, V.M. Vinosel, M.A. Janifer, S. Pauline, A. Manikandan, Effect of lattice strain on structure, morphology and magneto-dielectric properties of spinel NiGdxFe_2-xO_4 ferrite nano-crystallites synthesized by sol-gel route, J. Magn. Magn. Mater. 466 (2018) 238–251.
[30] M.V. Zdorovets, A.L. Kozlovskiy, Study of phase transformations in Co/$CoCo_2O_4$ nanowires, J. Alloy. Compd. 815 (2020) 152450.
[31] A. Malas, P. Pal, C.K. Das, Effect of expanded graphite and modified graphite flakes on the physical and thermo-mechanical properties of styrene butadiene rubber/polybutadiene rubber (SBR/BR) blends, Mater. Des. 55 (2014) 664–673.
[32] T. Chen, J. Cai, D. Gong, C. Liu, P. Liu, X. Cheng, D. Zhang, Facile fabrication of 3D biochar absorbers dual-loaded with Fe3O4 nanoparticles for enhanced microwave absorption, J. Alloy. Compd. 935 (2023) 168085, https://doi.org/10.1016/J.JALLCOM.2022.168085.
[33] H. Haham, J. Grinblat, M.T. Sougrati, L. Stievano, S. Margel, Engineering of Iron-Based magnetic activated carbon fabrics for environmental remediation, Materials 8 (2015) 4593, https://doi.org/10.3390/MA8074593.
[34] S. Goel, A. Garg, H.B. Baskey, M.K. Pandey, S. Tyagi, Studies on dielectric and magnetic properties of barium hexaferrite and bio-waste derived activated carbon composites for X-band microwave absorption, J. Alloy. Compd. 875 (2021) 160028, https://doi.org/10.1016/J.JALLCOM.2021.160028.
[35] A.P.G. Rodrigues, M.A. Morales, R.B. Silva, D.R.A.B. Lima, R.L.B.A. Medeiros, J. H. Araújo, D.M.A. Melo, Positive exchange bias effect in $LaCr_{0.5}Fe_{0.5}O_3$ perovskite, J. Phys. Chem. Solids 141 (2020) 109334.
[36] T. Blachowicz, A. Ehrmann, Exchange bias in thin Films—an update, Coatings 11 (2021) 122.
[37] D. Lisjak, A. Mertelj, Anisotropic magnetic nanoparticles: a review of their properties, syntheses and potential applications, Prog. Mater. Sci. 95 (2018) 286–328.
[38] I.A. Belyaeva, E.Y. Kramarenko, M. Shamonin, Magnetodielectric effect in magnetoactive elastomers: transient response and hysteresis, Polymers 127 (2017) 119–128, https://doi.org/10.1016/J.POLYMER.2017.08.056.
[39] V. Patsula, M. Moskvin, S. Dutz, D. Horák, Size-dependent Magnetic Properties of Iron Oxide Nanoparticles, (2015). 〈https://doi.org/10.1016/j.jpcs.2015.09.008〉.
[40] X.-R. Feng, X. Hou, Y.-C. Zheng, K. Jiang, J.-T. Liu, M. Wang, Defect engineering on carbon nanotubes or graphene to balance conduction and polarization loss for enhancing microwave absorption, ACS Appl. Nano Mater. (2024), https://doi.org/10.1021/ACSANM.4C06217.
[41] S. Mandal, Y. Hou, M. Wang, T.D. Anthopoulos, K.L. Choy, Surface modification of Hetero-phase nanoparticles for low-cost solution-processable High-k dielectric polymer nanocomposites, cite this, ACS Appl. Mater. Interfaces 15 (2023) 7371–7379, https://doi.org/10.1021/acsami.2c19559.
[42] A. Kusior, K. Michalec, P. Jelen, M. Radecka, Shaped Fe_2O_3 nanoparticles – synthesis and enhanced photocatalytic degradation towards RhB, Appl. Surf. Sci. 476 (2019) 342–352.
[43] G. Wu, Y. Cheng, Y. Ren, Y. Wang, Z. Wang, H. Wu, Synthesis and characterization of γ-Fe_2O_3@C nanorod-carbon sphere composite and its application as microwave absorbing material, J. Alloy. Compd. 652 (2015) 346–350.

[44] Y. Shu, T. Zhao, Y. Li, L. Yang, X. Li, G. Feng, W. Jia, F. Luo, Porous Fe/FeO/Fe_2O_3 nanorod/RGO composites with high-efficiency electromagnetic wave absorption property, Appl. Surf. Sci. 626 (2023) 157223.

[45] T. Govindasamy, N.K. Mathew, V.K. Asapu, V. Subramanian, B. Subramanian, Evaluating the microwave absorbing performance of polymer-free thin Fe_3O_4−MWCNT NCs in X-band region, Surf. Interfaces 44 (2024) 103716, https://doi.org/10.1016/J.SURFIN.2023.103716.

[46] X. Li, L. Wang, W. You, X. Li, L. Yang, J. Zhang, M. Wang, R. Che, Enhanced microwave absorption performance from abundant polarization sites of ZnO nanocrystals embedded in CNTs via confined space synthesis, Nanoscale 11 (2019) 22539–22549, https://doi.org/10.1039/C9NR07895A.

[47] B. Zhang, Y. Jiang, R. Balasubramanian, Synthesis, formation mechanisms and applications of biomass-derived carbonaceous materials: a critical review, J. Mater. Chem. A 9 (2021) 24759–24802.

[48] E. Ribeiro, G. Plantard, F. Teyssandier, F. Maury, N. Sadiki, D. Chaumont, V. Goetz, Activated-carbon/TiO2composites preparation: an original grafting by milling approach for solar water treatment applications, J. Environ. Chem. Eng. 8 (2020) 104115.

[49] E.C.T. Ba, M.R. Dumont, P.S. Martins, B. da Silva Pinheiro, M.P.M. da Cruz, J. W. Barbosa, Deconvolution process approach in Raman spectra of DLC coating to determine the sp^3 hybridization content using the ID/IG ratio in relation to the quantification determined by X-ray photoelectron spectroscopy, Diam. Relat. Mater. 122 (2022) 108818.

[50] S.M. Ansari, B.B. Sinha, D. Phase, D. Sen, P.U. Sastry, Y.D. Kolekar, C.V. Ramana, Particle size, morphology, and chemical composition controlled $CoFe_2O_4$ nanoparticles with tunable magnetic properties via oleic acid based solvothermal, ACS Publ. 2 (2019) 1828–1843.

[51] B. Wu, H.M. Tuncer, A. Katsounaros, W. Wu, M.T. Cole, K. Ying, L. Zhang, W. I. Milne, Y. Hao, Microwave absorption and radiation from large-area multilayer CVD graphene, Carbon N. Y 77 (2014) 814–822.

[52] M. Zhang, J. Zhang, H. Lin, T. Wang, S. Ding, Z. Li, J. Wang, A. Meng, Q. Li, Y. Lin, Designable synthesis of reduced graphene oxide modified using $CoFe_2O_4$ nanospheres with tunable enhanced microwave absorption performances between the whole x and ku bands, Compos. Part B 190 (2020) 107902.

[53] X. Zhang, X. Zhang, D. Liu, L. Wang, G. Wen, Y. Wang, X. Huang, Advances in carbon microsphere-based nanomaterials for efficient electromagnetic wave absorption, Langmuir 40 (2024) 18857–18881.

[54] M. Mahmoodi, B. Aslibeiki, R. Peymanfar, H. Naghshara, Oleaster seed-derived activated carbon/ferrite nanocomposite for microwave absorption in the X-band range, Front. Mater. 9 (2022) 1088196.

[55] S. Goel, A. Garg, H.B. Baskey, S. Tyagi, Microwave absorption study of low-density composites of barium hexaferrite and carbon black in X-band, J. Sol-Gel Sci. Technol. 98 (2021) 351–363.

[56] Z. Ji, Q. Wang, Z. Wang, Y. Duan, C. Dong, P.K. Liaw, Electromagnetic wave-absorbing behavior of soft-magnetic medium entropy alloys with BCC/L21 coherent microstructure, Mater. Des. 222 (2022) 111054.

[57] N. Yah, H. Rahim, Y. Lee, F. Wee, Electromagnetic wave absorption properties of novel Green composites coconut fiber coir and charcoal powder over X-band frequency for electromagnetic wave, Metaconf. Org. 7 (2018).

[58] X. Zeng, X. Cheng, R. Yu, G.D. Stucky, Electromagnetic microwave absorption theory and recent achievements in microwave absorbers, Carbon N. Y 168 (2020) 606–623, https://doi.org/10.1016/J.CARBON.2020.07.028.

[59] D. Xiang, Q. He, C. Fan, Y. Wang, X. Yin, C. Wang, Preparation and 3D network structure optimization of SiC and SiC@Fe_3Si nanofibers for enhanced electromagnetic wave absorption, Mater. Today Nano 30 (2025).

[60] D. Wu, S. Deng, Y. Wang, J. Wen, L. Ren, Q. He, Hierarchical porous carbon fibers for broadband and tunable high-performance microwave absorption, Mater. Res. Bull. 172 (2024).

[61] H.P. Hari, E. Jayamani, K.H. Soon, Y.C. Wong, M.R. Rahman, M.K. Bin Bakri, Interfacial polarization effects on dielectric properties in flax reinforced polypropylene/strontium titanate composites, Mater. Chem. Phys. 265 (2021) 124489.

[62] B. Quan, X. Liang, G. Ji, Y. Cheng, W. Liu, J. Ma, Y. Zhang, D. Li, G. Xu, Dielectric polarization in electromagnetic wave absorption: review and perspective, J. Alloy. Compd. 728 (2017) 1065–1075.

[63] E.C. Abenojar, S. Wickramasinghe, J. Bas-Concepcion, A.C.S. Samia, Structural effects on the magnetic hyperthermia properties of iron oxide nanoparticles, Prog. Nat. Sci. Mater. Int. 26 (2016) 440–448.

[64] X. Zuo, H. Ding, J. Zhang, T. Fang, D. Zhang, Carbothermal treated iron oxide nanoparticles with improving magnetic heating efficiency for hyperthermia, Results Phys. 32 (2022) 105095.

[65] M. Hammad, S. Hardt, B. Mues, S. Salamon, J. Landers, I. Slabu, H. Wende, C. Schulz, H. Wiggers, Gas-phase synthesis of iron oxide nanoparticles for improved magnetic hyperthermia performance, J. Alloy. Compd. 824 (2020) 153814.

[66] S. Goel, M. Bala, A. Garg, V.D. Shivling, S. Tyagi, Lanthanum doped barium hexaferrite nanoparticles for enhanced microwave absorption, Mater. Today Proc. 28 (2020) 1753–1758.

[67] S. Goel, A. Tyagi, A. Garg, S. Kumar, H.B. Baskey, R.K. Gupta, S. Tyagi, Microwave absorption study of composites based on CQD@$BaTiO_3$ core shell and $BaFe_{12}O_{19}$ nanoparticles, J. Alloy. Compd. 855 (2021) 157411.

[68] J. Luo, I. Mahariq, K.Y. You, S. Mehrez, M. Fayed, S. Alamri, Optimizing the layer arrangement in a three-layer absorber based on magneto-electric nanocomposite for enhanced microwave absorption, Ceram. Int. 48 (2022) 31537–31547.

[69] Y. Huang, W.L. Song, C. Wang, Y. Xu, W. Wei, M. Chen, L. Tang, D. Fang, Multi-scale design of electromagnetic composite metamaterials for broadband microwave absorption, Compos. Sci. Technol. 162 (2018) 206–214.

[70] P. Kaur, S. Bindra Narang, S. Bahel, Complex permittivity, complex permeability and reflection loss of Co-Zr substituted La-Sr hexaferrites in 18–40 GHz frequency range, J. Magn. Magn. Mater. 502 (2020) 166456.

[71] Y. Zhang, H. Dong, C. Yu, Z. Wang, Y. Huang, Metastructure based broadband structural stealth with material-structure-function integration, Compos. Sci. Technol. 253 (2024) 110661.

[72] D. Tahir, H. Heryanto, S. Ilyas, A.N. Fahri, R. Rahmat, M.H. Rahmi, Y. Taryana, S. G. Sukaryo, Excellent electromagnetic wave absorption of Co/Fe_2O_3 composites by additional activated carbon for tuning the optical and the magnetic properties, J. Alloy. Compd. 864 (2021) 158780.

[73] J. Wang, J. Wang, R. Xu, Y. Sun, B. Zhang, W. Chen, T. Wang, S. Yang, Enhanced microwave absorption properties of epoxy composites reinforced with $Fe_{50}Ni_{50}$-functionalized graphene, J. Alloy. Compd. 653 (2015) 14–21, https://doi.org/10.1016/J.JALLCOM.2015.08.278.

[74] Y. Li, D. Li, J. Yang, H. Luo, F. Chen, X. Wang, R. Gong, Enhanced microwave absorption and surface wave attenuation properties of $Co_{0.5}Ni_{0.5}Fe_2O_4$ Fibers/Reduced graphene oxide composites, Materials 11 (2018) 508.

[75] B. Quan, X. Liang, G. Xu, Y. Cheng, Y. Zhang, W. Liu, G. Ji, Y. Du, A permittivity regulating strategy to achieve high-performance electromagnetic wave absorbers with compatibility of impedance matching and energy conservation, N. J. Chem. 41 (2017) 1259–1266.

[76] I. Ismail, I.R. Ibrahim, K.A. Matori, Z. Awang, M.M. Muhammad Zulkimi, F. Mohd Idris, R. Nazlan, R.S. Azis, M.H. Mohd Zaid, S.N.A. Rusly, M. Ertugrul, Comparative study of single- and double-layer $BaFe_{12}O_{19}$-Graphite nanocomposites for electromagnetic wave absorber applications, Mater. Res. Bull. 126 (2020) 110843.

[77] X. Huang, J. Zhang, M. Lai, T. Sang, Preparation and microwave absorption mechanisms of the NiZn ferrite nanofibers, J. Alloy. Compd. 627 (2015) 367–373.

[78] Y. Shi, H. Jing, B. Liu, H. Qian, Electromagnetic (EM) wave absorption properties of cementitious building composites containing MnZn ferrite: preferable effective bandwidth and thickness via iron and graphite addition, J. Magn. Magn. Mater. 560 (2022) 169555.

[79] F. Cao, F. Yan, J. Xu, C. Zhu, L. Qi, C. Li, Y. Chen, Tailing size and impedance matching characteristic of nitrogen-doped carbon nanotubes for electromagnetic wave absorption, Carbon N. Y 174 (2021) 79–89.

[80] C. Jia, T. Xia, Y. Ma, N. He, Z. Yu, Z. Lou, Y. Li, Fe_3O_4/α-Fe decorated porous carbon-based composites with adjustable electromagnetic wave absorption: impedance matching and loading rate, J. Alloy. Compd. 858 (2021) 157706, https://doi.org/10.1016/J.JALLCOM.2020.157706.

[81] B. Zhao, J. Deng, L. Liang, C. Zuo, Z. Bai, X. Guo, R. Zhang, Lightweight porous Co_3O_4 and Co/CoO nanofibers with tunable impedance match and configuration-dependent microwave absorption properties, CrystEngComm 19 (2017) 6095–6106.

[82] V.A. Zhuravlev, R.M. Minin, V.I. Itin, Y.M. Lopushnyak, A.V. Zhuravlev, E. P. Lilenko, Study of the Magnetic Anisotropy of the Multiphase Samples of the Ferrimagnets with Hexagonal Crystal Structure by the Method of Ferromagnetic Resonance. IOP Conf. Ser. Mater. Sci. Eng., Institute of Physics Publishing, 2017 012081.